Complex Diffusion on Scalar and Vector Valued Image Graphs*

Dohyung Seo[1] and Baba C. Vemuri[2]

[1] Department of Electrical and Computer Engineering (ECE)
University of Florida, USA
dhseo@ufl.edu
[2] Department of Computer and Information Science and Engineering (CISE)
University of Florida, USA
vemuri@cise.ufl.edu

Abstract. Complex diffusion was introduced in the image processing literature as a means to achieve simultaneous denoising and enhancement of scalar valued images. In this paper, we present a novel geometric framework to achieve complex diffusion for color images represented by image graphs. In this framework, we develop a novel variational formulation that involves a modified harmonic map functional and is quite distinct from the Polyakov action described by Sochen et al. Our formulation provides a novel framework for simultaneous feature preserving denoising and enhancement. We also develop a quaternionic diffusion that can be applied to color image data represented by a quaternion in the image graph framework. In this framework, the real and imaginary parts can be interpreted as low and high-pass filtered data respectively. Finally, we suggest novel ways to use the imaginary part of complex diffusion toward image reconstruction. We present results of comparison between the complex diffusion, quaternionic diffusion and the well known Beltrami flow in the image graph framework.

1 Introduction

Image denoising is a quintessential component of most image analysis tasks and there are numerous denoising methods reported in the literature. In the past few decades, methods based on partial differential equations (PDEs) have become very popular. Some of the PDE-based methods are derived from minimization principles while others are not. The general mathematical form of a feature preserving anisotropic diffusion is given by

$$\frac{\partial I}{\partial t} = Div(g(|\nabla u|)\nabla u)$$

Here, $u(x, y; t)|_{t=0} = I(x, y)$ is the function being smoothed. The choice of $g(|\nabla u|)$ in the above leads to various types of diffusion flows.

* This research was supported in part by the NIH grant NS46812.

D. Cremers et al. (Eds.): EMMCVPR 2009, LNCS 5681, pp. 98–111, 2009.

Alternatively, one may represent the 2D image as a graph by embedding it in R^3, as a surface Σ with local coordinates (σ^1, σ^2). The embedding map X is given by, $X : (\sigma^1, \sigma^2) \rightarrow (x, y, I(x, y))$. This provides a geometric interpretation to the PDEs as those that modify some geometric property such as area of the 2D manifold representing the image surface. In the case of vector-valued images, the embedding map X is given by, $X : (\sigma^1, \sigma^2) \rightarrow (x, y, I^i(\sigma^1, \sigma^2))$, where, $I^i(x, y)$ are the channels of the given vector-valued image, and the $2+i$ dimensional manifold, $(x, y, I^i(\sigma^1, \sigma^2))$ is refered to as the space-feature manifold, M [2]. This graph representation also provides a geometric way to handle the interaction between the components (channels) of the vector-valued images. Kimmel et al., [1,2,3] pioneered the use of image graph representation to perform image smoothing in scalar and vector-valued image data sets. They introduced the Polyakov action [4] to derive various flows such as the Beltrami, mean curvature, and the Perona-Malik flows. One of the benefits of this approach is that the channels in multi-channel (vector-valued) images such as color images can be correlated in a geometrical way. Diffusing the RGB channels in a color image while retaining their correlation is essential. If we perform isotropic or anisotropic diffusion of each channel independently, all correlations are ignored and the solution would be erroneous.

Alternatively, one may simply extend the traditional diffusion to the complex-domain, which was pioneered by Gilboa et al. [5,6,7]. In complex diffusion, an image, $I(x, y)$, which is a real-valued function in general, is extended to the complex domain, i.e., $I(x, y) = I_R(x, y) + iI_M(x, y)$. Then, the isotropic diffusion equation is generalized to, $I = C\triangle I$ where, C is a complex number with unit norm $e^{i\theta}$, and $\triangle$ is defined as usual by $\frac{\partial^2}{\partial x^2} + \frac{\partial^2}{\partial y^2}$.

More generally, diffusion equations are given by

$$\frac{\partial I}{\partial t} = H(t)I \tag{1}$$

where $H(t)$ is a diffusion operator which can be either isotropic or anisotropic and can produce linear or nonlinear scale-spaces respectively. In the case of complex diffusion, $H(t)$ is a complex operator and can be rewritten as follows:

$$H(t) = H_R(t) + iH_M(t) = e^{i\theta}h(t) \tag{2}$$

where $h(t)$ is a real-valued operator. Then, the diffusion equations for the real and imaginary parts are given by

$$\frac{\partial I_R}{\partial t} = \cos(\theta)h(t)I_R - \sin(\theta)h(t)I_M \tag{3}$$

$$\frac{\partial I_M}{\partial t} = \sin(\theta)h(t)I_R + \cos(\theta)h(t)I_M. \tag{4}$$

The processed input image is considered as a solution to Eq.(3). In the case of isotropic diffusion, $h(t)$ becomes the $\triangle$ operator. Gilboa et al. showed that small positive values of θ lead to approximating the real part of I by the regular

isotropic diffusion and the imaginary part by the smoothed second derivative of the real part. This allows one to achieve denoising and enhancement simultaneously. Therefore, regular (non-complex) diffusions discussed in the previous paragraphs can be seen as special cases of complex diffusions. Because the imaginary part represents the smoothed second derivative of the real part, the imaginary part contains the edge information of the real part. They applied this aspect of the imaginary part to denoise and enhance the images. For the task of denoising, they introduced a new anisotropic diffusion by replacing $|\nabla u|$ in $g(|\nabla u|)$ of Perona-Malik diffusion with that of the imaginary part as follows:

$$\frac{\partial I}{\partial t} = \nabla \cdot \left(\frac{e^{i\theta}}{1 + \left(\frac{I_M}{k\theta}\right)^2} \nabla I \right) \tag{5}$$

where I_M is the imaginary part of the complex image I and k is a threshold parameter. This allowed the diffusion flow to avoid the stair-casing effect. They also introduced a shock filter which used the imaginary part as edge information. However, they did not apply the complex diffusion model to multi-channel images and did not suggest a method to account for the coupling of the channels. *In this paper, we present a novel model for simultaneous smoothing and enhancement by mapping the real and complex channels to* $\boldsymbol{C}^n$*, introducing an image-surface metric and constructing an action functional distinct from the Polyakov action in [1].* In our approach, the correlation between the color channels (R, G and B) is introduced via the metric on the image graph manifold. Additionally, we applied our action functional to the quaternion representation of a color image in the graph representation. Liu et al.[8] have suggested a way to treat the color channels as a quaternion assuming that the R,G, and B channels were correlated through the quaternion algebra. In this approach, the R,G, and B were mapped to the pure quaternion parts with one extra dimension, which was the real part of the quaternion representation.

We present several experimental results depicting the performance of our model in comparison to the complex diffusion model of Gilboa et al. [5], for the scalar image denoising and enhancement case as well as with the Beltrami flow [2] for color image denoising. The rest of this paper is organized as follows. In Section 2, we present a novel metric for the complex image manifold and a novel functional whose minimization yields the desired flow equation. This is followed by a description of the quaternion representation for color images, a novel formulation of the functional and the accompanying flow equation for color image denoising and enhancement. In Section 3, we present experimental results for our model applied to color images along with comparisons to other models. In Section 3.2, we describe techniques to reduce computational time by considering the diffusion of the real part as a low-pass filter and the imaginary part as high-pass filter, and adding these two parts for the denoised reconstruction. In Section 4, we demonstrate that this reconstruction method can be applied to achieve high quality reconstruction. We draw conclusions in Section 5.

2 Action Formalism for Complex Diffusion

In this section, we introduce a metric for the complex image manifold for multi-channel images, and construct an action functional that is minimized to derive the complex diffusion equation. In addition, we applied the metric and the action functional to the quaternion representation of RGB images.

2.1 The Image Metric

The general idea of complex diffusion has been investigated in [5]. However, their primary focus was on gray level images. There was no description of extensions to vector-valued data sets. Since we deal with processing of multi channel images here, the key challenges involve processing the vector-valued data and capturing the correlation between the channels. In [1,2], a norm functional called the Polyakov action [4] and an embedding map $\mathbf{X} : \Sigma \rightarrow \mathbf{R}^n$ were introduced, where Σ is a 2-D manifold. They were used to capture the interaction between the multiple channels, and minimize the norm functional to obtain specific flows that smooth images in different ways. In this paper, we suggest an alternative to the Polyakov action, where the image manifold, Σ, is mapped to an n-dimensional complex manifold by $\mathbf{Z} : \Sigma \rightarrow \mathbf{C}^n$. Upon denoting the local coordinates on the 2-D manifold Σ by (σ_1, σ_2), the map $\mathbf{Z}$ is given by $[Z^1(\sigma^1, \sigma^2), Z^2(\sigma^1, \sigma^2), ..., Z^n(\sigma^1, \sigma^2)]$, where all the Z's are complex-valued. For example, a color (RGB) image can be mapped by $\mathbf{Z}$ as follows:

$$\mathbf{Z} : (\sigma^1, \sigma^2) \rightarrow [z^1, \bar{z}^1, Z^l = I^l(\sigma^1, \sigma^2), \bar{Z}^l] \tag{6}$$

where $z = \sigma^1 + i\sigma^2$, $\bar{z}$ is the complex conjugate of z, I^l is a complex-valued channel, $I^l_R(\sigma^1, \sigma^2) + iI^l_M(\sigma^1, \sigma^2)$, $\bar{Z}^l$ is the complex conjugate of Z^l and the index l runs over R,G, and B.

Let M, the space-feature manifold denote the embedding manifold of the complex image graph, with the map $\mathbf{Z} : \Sigma \rightarrow M$. Let $g_{\mu\nu}$ be the metric on the image manifold, Σ, and h_{ij} be the metric on M. Here, h_{ij} is defined such that $h_{ij}dZ^i dZ^j$ gives a length element on M, and this metric makes the manifold M a Riemannian manifold with $(n \times 2) + 2$ dimensions ,where n is the number of channels and the local spatial coordinates are represented by two additional dimensions. For a gray level image, h_{ij} becomes

$$h = \begin{pmatrix} 0 & \frac{1}{2} & 0 & 0 \\ \frac{1}{2} & 0 & 0 & 0 \\ 0 & 0 & 0 & \frac{1}{2} \\ 0 & 0 & \frac{1}{2} & 0 \end{pmatrix} \tag{7}$$

so that the length element is $dzd\bar{z} + dId\bar{I} = (d\sigma^1)^2 + (d\sigma^2)^2 + dI^2_R + dI^2_M$. Then, the image metric, $g_{\mu\nu}$ is given explicitly as follow:

$$g_{\mu\nu}(\sigma^1, \sigma^2) = h_{ij}(\mathbf{Z})\partial_\mu Z^i \partial_\nu Z^j \tag{8}$$

where, $\partial_\mu Z^i = \partial Z^i / \partial \sigma_\mu$. The image metric for the n-channel case is given explicitly by,

$$g_{\mu\nu} = \begin{pmatrix} 1 + \sum_{l=1}^{n} I_x^l \bar{I}_x^l & \frac{1}{2}\sum_{l=1}^{n}(I_x^l \bar{I}_y^l + I_y^l \bar{I}_x^l) \\ \frac{1}{2}\sum_{l=1}^{n}(I_x^l \bar{I}_y^l + I_y^l \bar{I}_x^l) & 1 + \sum_{l=1}^{n} I_y^l \bar{I}_y^l \end{pmatrix} \tag{9}$$

where x and y are the spatial coordinates. We are now ready to present the action formalism.

2.2 The Action Formalism

Images in computer vision are usually real-valued. Therefore, it is natural to pose them as a real-valued graph with a real-valued metric. However, in this paper we seek an action appropriate for complex-valued functions and one that is distinct from the Polyakov action presented in [2]. We would like the gradient descent (flow) equation of the new action to match the complex diffusion introduced in [5] under a special geometry and depict edge-preserving flows on a graph. We propose a specific action for n-channel images satisfying the conditions above, given by:

$$S = \int\int \boldsymbol{F}(z, \bar{z}, I_x^l, l_y^l \bar{I}_x^l, \bar{I}_y^l)\sqrt{g}dxdy \tag{10}$$

$$\boldsymbol{F} = \frac{1}{2}\sum_{l=1}^{n}(\nabla I^l \cdot \nabla I^l e^{l\theta_l} + \nabla \bar{I}^l \cdot \nabla \bar{I}^l e^{-l\theta_l}). \tag{11}$$

Here, x and y are local coordinates, and g is the determinant of the image metric $g_{\mu\nu}$, Eq.(9). In Eq.(10) and Eq.(11), I is complex image, $I_R + iI_M$ and $\bar{I}$ is its complex conjugate. In Eq.(11), generally, we can assign different phase θ_l to each channel. Setting g equal to the identity matrix and minimizing Eq.(10) by applying calculus of variation to Eq.(10), we can derive the isotropic complex diffusion equation introduced in [5] and details are given in following paragraphs.

We derive the gradient descent of Eq. (10) by evaluating the Euler-Lagrange equation with respect to the embedding. For this, we fix the x and y coordinates or z and $\bar{z}$, and vary the action with respect to I [2]. Then, the flow equation for I^l is given by:

$$\frac{\partial I^l}{\partial t} = \frac{1}{g^\beta}\left[\frac{d}{dx}\left(\frac{P^l}{\sqrt{g}}\right) + \frac{d}{dy}\left(\frac{Q^l}{\sqrt{g}}\right)\right] \tag{12}$$

where, P^l and Q^l are defined as:

$$P^l = g\frac{\partial F}{\partial I_x^l}, \qquad Q^l = g\frac{\partial F}{\partial I_y^l}. \tag{13}$$

In Eq.(12), we multiply the right hand side of the equation by a positive function, $1/(g^\beta)$, that will produce nonlinear scale-space and keep the flow geometrical as

suggested in [2]. The exponent β will be discussed subsequently. When β is large, the flow becomes more sensitive to edges. Eq.(12) can now be rewritten as follows:

$$\frac{\partial I^l}{\partial t} = \frac{1}{g^{(\beta+0.5)}} \left[P^l_x + Q^l_x - \frac{1}{2g}(g_x P^l + g_y Q^l) \right]. \tag{14}$$

Here, I^l, P^l and Q^l are complex valued defined as: $I^l(x,y) = I^l_R(x,y) + iI^l_M(x,y)$, $P^l(x,y) = P^l_R(x,y) + iP^l_M(x,y)$, and $Q^l(x,y) = Q^l_R(x,y) + iQ^l_M(x,y)$, where l is a channel index. As a special case, we can easily obtain the isotropic complex diffusion equation introduced in [5], by applying Eq. (10) to gray scale images and setting the metric $g_{\mu\nu}$ to be the identity matrix. Then, g is equal to 1, $I(x,y) = I_R(x,y) + iI_M(x,y)$, and the Eq. (11) becomes

$$\boldsymbol{F} = \cos\theta(|\nabla I_R|^2 - |\nabla I_M|^2) - 2\sin\theta(I_{Rx}I_{Mx} + I_{Ry}I_{My}) \tag{15}$$

The gradient descent of Eq.(14) results in the following flow equations:

$$\frac{\partial I_R}{\partial t} = cos(\theta)\triangle I_R - sin(\theta)\triangle I_M \tag{16}$$

$$\frac{\partial I_M}{\partial t} = sin(\theta)\triangle I_R + cos(\theta)\triangle I_M. \tag{17}$$

Here, we recover the complex isotropic diffusion introduced in [5]. There is no imaginary part in the initial condition of complex image I, and the target image is assigned to the real part of the initial condition. However, we can create an imaginary part from a non-zero theta via the time iteration of Eq.(14).

Another special case of Eq.(10) is obtained by setting θ equal to zero in Eq.(15) with same g and initial conditions as before. In this case, $\boldsymbol{F}$ reduces to $|\nabla I_R|^2$ and the gradient descent of Eq.(14) recovers the ordinary isotropic diffusion equation: $\frac{\partial I}{\partial t} = \triangle I$, $(I = I_R)$.

In Fig.1, we have compared the results of anisotropic diffusion using Eq.(14) with isotropic diffusion obtained using Eq.(16) and Eq.(17) and anisotropic diffusion from Eq.(5) when applied to a gray-level image. Fig.1(a) is the given input image and also the real part of the initial complex image. We can observe that Fig.1(h) has no blurring across edges compared to Fig.1(f) and is smoother than Fig.1(g). The real part of Eq.(5) is less smooth than others for θ larger than 5 degrees.

2.3 Quaternion Representation for Color Images

The geometric coupling of channels in the RGB image via the image metric term is not the only way to achieve the coupling. Labunets [9] suggested applying hypercomplex techniques to multi-channel images. He considered R,G, and B color channels as a triplet number. In his framework, color space is identified with the so-called triplet algebra. Instead of the triplet representation of color, Liu et al. [8] employed quaternion to represent the color channels. They considered the diffusion of quaternion images as an extension to the diffusion of

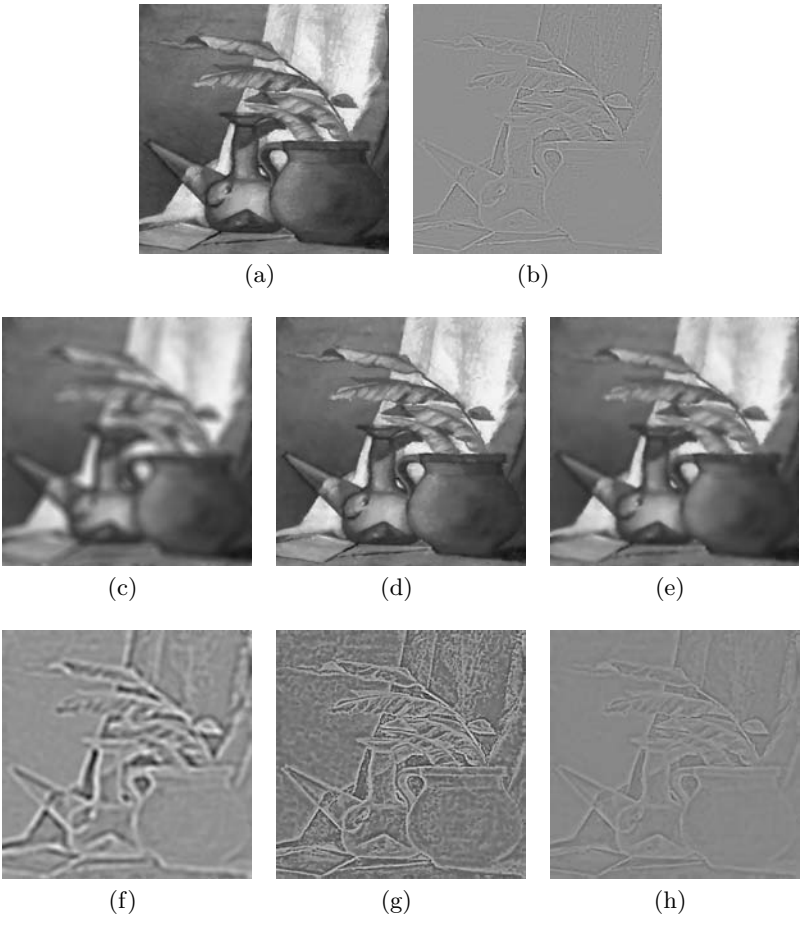

Fig. 1. (a) original image. (b) after one iteration of isotropic complex diffusion. (c) and (f) real and imaginary parts of (a) obtained by isotropic complex diffusion. (d) and (g) real and imaginary parts of (a) obtained using Eq.(5) with $k = 2$. (e) and (h) real and imaginary parts of (a) using Eq.(14) with $\beta = 5/6$. 100 time iterations have been processed with step size, 0.1 and $\theta = \pi/3$. All imaginary parts have been rescaled to 8-bit images for display.

complex images, and discussed the isotropic and anisotropic diffusion of quaternion valued RGB image. One of the choices of mapping RGB channels to a quaternion is to map R, G and B channels to pure quaternion parts, introducing an extra dimension which corresponds to real parts of quaternion, Then the quaternion of RGB channels, Q is represented by $Q = Q_0 + \mathbf{i}R + \mathbf{j}G + \mathbf{k}B$. Here, we introduce a novel geometric approach to achieve smoothing and enhancement of color images using the quaternions based representation of RGB, $[q, \bar{q}, Q, \bar{Q}]$, where $q = \sigma_1 + \mathbf{i}\sigma_2 + \mathbf{j}0 + \mathbf{k}0$. *We emphasize that this representation has never been*

used earlier and is indeed novel. The second and third components of the pure quaternion parts of q are fixed to zero. For the action formulation, Eq. (10), we choose Eq. (9) as the image metric after replacing z and I with q and Q respectively,

$$g_{\mu\nu} = \begin{pmatrix} 1 + Q_x\bar{Q}_x & \frac{1}{2}(Q_x\bar{Q}_y + Q_y\bar{Q}_x) \\ \frac{1}{2}(Q_x\bar{Q}_y + Q_y\bar{Q}_x) & 1 + Q_y\bar{Q}_y \end{pmatrix}, \tag{18}$$

The functional $\boldsymbol{F}$ in Eq. (11) must now be rewritten using the quaternion algebra as follows:

$$\boldsymbol{F} = \frac{1}{2}((\nabla Q \cdot \nabla Q)C + \bar{C}(\nabla\bar{Q} \cdot \nabla\bar{Q})) \tag{19}$$

Here, C is a quaternion coefficient defined as $e^{\mathbf{e}_\phi\theta_\phi} = cos\theta_\phi + \mathbf{e}_\phi sin\theta_\phi$, and $\mathbf{e}_\phi = \mathbf{i}C_R + \mathbf{j}C_G + \mathbf{k}C_B$, where $C_R^2 + C_G^2 + C_B^2 = 1$ [10], and $\bar{C}$ is the quaternion conjugate of C. Then, we can have the flow equation, Eq.(14) for quaternion RGB by replacing Eq.(13) with

$$P^i = g\frac{\partial F}{\partial Q_x^i}, \qquad Q^i = g\frac{\partial F}{\partial Q_y^i} \tag{20}$$

where $Q^i \in \{I_0, R, G, B\}$. The correlation between the channels are introduced via a quaternion multiplication between $Q(\bar{Q})$ and $C(\bar{C})$ [8] as well as the metric on the image (graph) manifold. When we set $g_{\mu\nu}$ to the identity metric as we have done previously, and $C_R = C_G = C_B = 1/\sqrt{3}$, we have the isotropic diffusion of the color image in the quaternion framework presented in [8]:

$$\frac{dI_0}{dt} = \cos\theta_\phi \triangle I_0 - \sin\theta_\phi \frac{1}{\sqrt{3}} \triangle (R + G + B), \tag{21}$$

$$\frac{dQ^i}{dt} = \cos\theta_\phi \triangle Q^i + \sin\theta_\phi \frac{1}{\sqrt{3}} \triangle (I_0 + Q^j - Q^k), \tag{22}$$

where i,j and k follow the cyclic permutation of R,G and B. When θ_ϕ is negative, Eq.(21) will have a form similar to that of Eq.(17). This implies that the scalar part of the quaternion diffusion will capture the smoothed second order of $(R+G+B)/\sqrt{3}$ [8]. Additionally, recalling that correlation between channels is introduced only by the image metric, Eq.(9) in the case of complex diffusion, we can recognize that the quaternion algebra introduces alternative type of correlation between channels in Eq.(22).

3 Denoising and Edge Enhancement Experiments

In this paper, we apply our method to noisy color images using an image graph representation. There are two parameters in our model: the exponent β in Eq.(14) and θ in Eq.(11). In [5], large values of phase, θ, made edges represented by the imaginary part thicken with increasing iterations, and small θ less than 5 degrees was recommended for isotropic and anisotropic diffusion to retain sharp

edges. In contrast, in our work here, large phase values increase the magnitude of the imaginary part and slow down diffusion speed near edges, which prevent thick edges due to large θ. The exponent, β of the non-linear scale multiplier influences the diffusion flows geometrically. For example, the diffusion equations from Polyakov action with different β values results in different flows like the Beltrami flows, Panora-Malik flows, Mean curvature flows and others [2,11]. The main purpose of this multiplicative factor is to achieve edge-preserving denoising. In this paper, we choose β from the interval $[0.5, 1]$. These two free parameters are chosen empirically based on the amount of noise in the data.

3.1 Denoising Experiments

The results of denoising depend on parameters, θ and β, similar to the earlier approaches [2,5]. The optimal parameter values depend on the amount of noise. The larger phase angles, θ and βs, lead to diffusions that are more sensitive to edges. We have applied the complex RGB flow and the quaternion flow to color images with added Gaussian noise, and compared the results with Beltrami flow. Our test image had an additive Gaussian noise of 25.3dB. Fig.2(a) and Fig.2(b) show original image and the noisy version respectively. We used the peak SNR (PSNR) as the stopping criteria for iterations. We stopped the iterations when the denoised images reached the maximum PSNR. Fig.2(c) and Fig.2(d) show denoised images obtained using the complex (RGB) flow with $\theta = 7\pi/30$ and $\beta = 5/6$, and the quaternionic flow with $\theta_\phi = -7\pi/30$,$\beta = 5/6$ and $C_R = C_G = C_B = 1/\sqrt{3}$. All the experiments reported here were implemented in Matlab 2007a, on an Intel Core Duo 2.16GHz CPU. The step size of time iteration is 0.1. We achieved the denoising using the complex (RGB) flow with a maximum PSNR of 26.6 dB in 38.6 seconds. Similarly, for the quaternionic flow the maximum PSNR is 26.5 dB and the processing time is 27.8 seconds. Fig.2(e) shows a denoised image using Beltrami flow with maximum PSNR of 25.4 dB and a processing time of 13.8 seconds (76 iterations). The result of the complex flow depicts higher degree of smoothing than that due to the Beltrami flow. When the noise is in the image detail, Beltrami flow tends to confuse the noise as detail, and this effect slows down diffusion velocity locally. Fig.2(f) shows the denoised image using Beltrami flow after a processing time of 89.8 secs. (500 iterations). The result is still noisy even after several iterations compared with the results from complex diffusion. The complex diffusion and quaternion diffusion yield results comparable to each other in quality, and are better than the Beltrami flow. However, the quaternion diffusion required less processing time compared to the complex diffusion case. This is due to the fact that the quaternion representation is 6-dimensional when using an RGB color image graph, where as the complex diffusion of the RGB image graph is 8-dimensional. Fig.3 shows imaginary parts of Figures 2(a)-2(d). Fig.3(a) and Fig.3(b) have been achieved after just one iteration on Fig.2(a) and Fig.2(b) respectively. We can see that the imaginary parts are also smoothed along with their corresponding real parts, which we consider as the processed images of the target image.

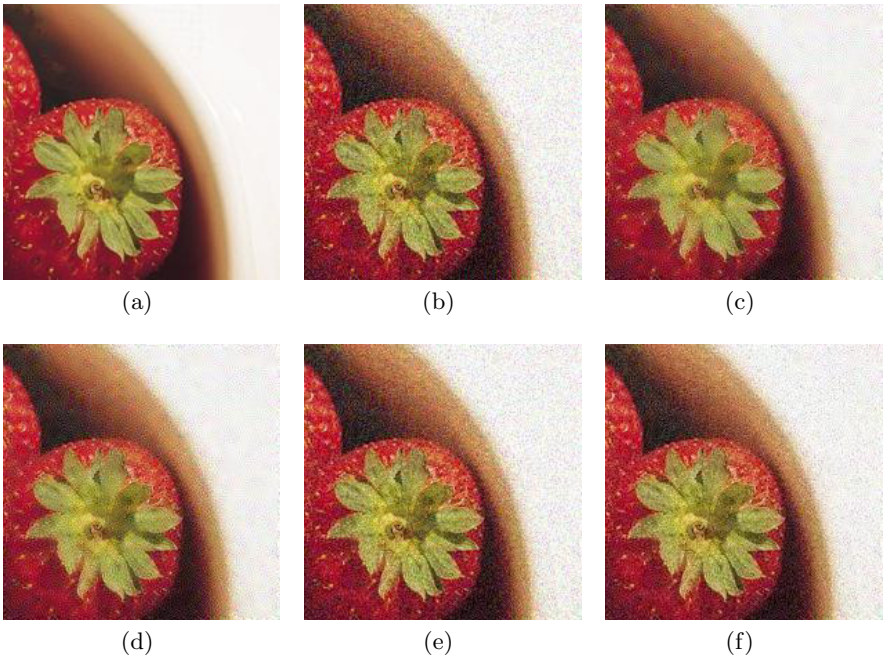

Fig. 2. (a) and (b) an original image and the image with the Gaussian noise of peak SNR 25.3dB respectively. (c) denoised image using complex RGB flows. (d) denoised image using quaternionic flows. The parameters are $\theta = 7\pi/30$ and $\beta = 5/6$ and the three pure quaternion components are $1/\sqrt{3}$. (e) and (f) images obtained using Beltrami flows with different processing times.

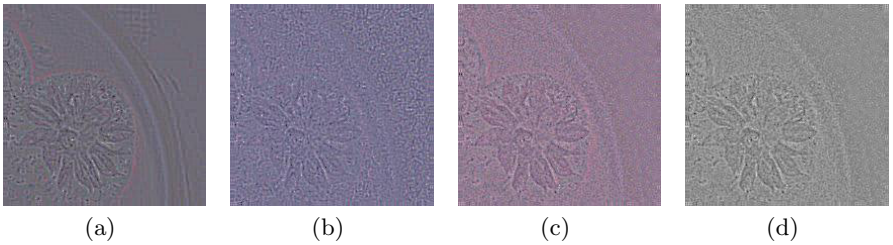

Fig. 3. (a) Imaginary part of Fig.2(a). (b) Imaginary part of Fig.2(b). (c) and (d) imaginary parts corresponding to Fig.2(c) and Fig.2(d) respectively (a) and (b) have been achieved after one iteration. All images are rescaled to 8-bit images for display.

3.2 Image Reconstruction

Recall that the imaginary part of complex diffusion corresponds to the smooth second order derivative and the real part corresponds to smoothed image. Hence, it is very natural to consider the imaginary part as a high-pass filter and the real

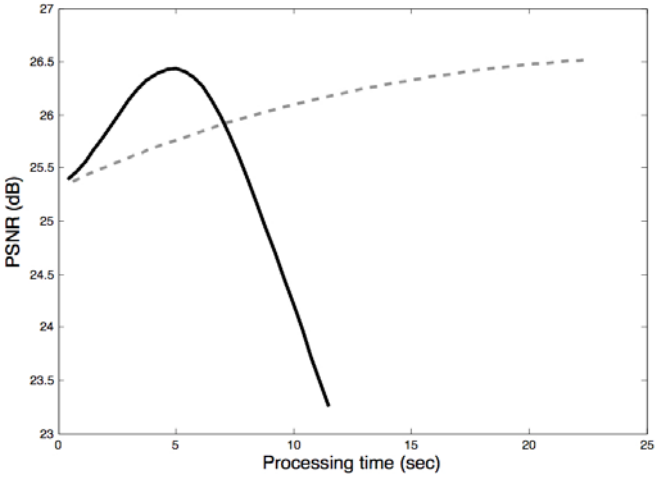

Fig. 4. Gray dashed line: PSNR of a denoised image by Eq. (14) without the reconstruction. Black solid line: PSNR with the reconstruction. The maxima of the black and gray lines are 26.44 dB and 26.57 dB respectively.

part as a low-pass filter, and think of addition of these two parts to recover original image which is an enhanced version of the original and contains smoothed edges. This process is similar to the image reconstruction via wavelet transformation, in which we add the lowest resolution version of low-pass filtered image with a sequence of high pass filtered images from the lowest resolution up to the desired resolution. However, we add the real part (low pass-filtered version) to the imaginary part (high pass-filtered version) so as to recover the smoothed and enhanced original image. (θ must always be positive, the reason for which will be explained in next section.) If we update the real parts by this addition after every iteration, the image can be denoised by diffusion as well as achieve reconstruction. To see this in detail, we discretize Eq.(3) and Eq.(4) in time, as follows:

$$I_R^{i+1} = I_R^i + \Delta t(\cos\theta h^i I_R^i - \sin\theta h^i I_M^i) \tag{23}$$

$$I_M^{i+1} = I_M^i + \Delta t(\sin\theta h^i I_R^i + \cos\theta h^i I_M^i) \tag{24}$$

Here, Δt is the time-step size of the iteration. Then we can evaluate I_R and I_M after i iterations, by a recursive relation :

$$I_R^{i+1} = I_R^0 + \Delta t \sum_{j=0}^{i} (\cos\theta h^j I_R^j - \sin\theta h^j I_M^j), \tag{25}$$

$$I_M^{i+1} = I_M^0 + \Delta t \sum_{j=0}^{i} (\sin\theta h^j I_R^j + \cos\theta h^j I_M^j). \tag{26}$$

Here, I_{M0} is set to be zero. However, if we reset the real part to a sum of the imaginary and real part so as to obtain a reconstruction ($I_R^{i+1} \rightarrow I_R^{i+1} + I_M^{i+1}$) after each iteration (and before next iteration), Eq.(23) can be rewritten as,

$$I_R^{i+1} = I_R^i + I_M^i + \Delta t((\cos\theta + \sin\theta)h^i I_R^i + (\cos\theta - \sin\theta)h^i I_M^i), \tag{27}$$

Rewriting Eq.(25) using Eq.(27) gives us the following recursive relationship:

$$I_R^{i+1} = I_R^0 + \sum_{j=0}^{i} I_M^j + \Delta t \sum_{j=0}^{i}((\cos\theta + \sin\theta)h^j I_R^j + (\cos\theta - \sin\theta)h^j I_M^j). \tag{28}$$

noise with 25.3dB PSNR. The gray dashed line in Fig.4 represents the PSNR results obtained by applying Eq. (14) without the reconstruction, and the black solid line in Fig.4 represents PSNR results with the reconstruction. The maxima of the black and gray line are 26.44 dB and 26.57 dB respectively. We can see that the reconstruction at each iteration is improves the smoothing process. This test was done with the parameter values: $\beta = \frac{5}{6}$ and $\theta = \frac{\pi}{6}$.

Fig. 5. (a) Original image. (b) and (c) Enhanced images with $\beta = 1/2$, $\theta = -\pi/6$ and $\theta = -\pi/3$ respectively after 16 iterations. (d) and (e) Enhanced images with $\beta = 5/6$, $\theta = -\pi/6$ and $\theta = -\pi/3$ respectively after 20 iterations. (f) Enhanced image with same parameters after 25 iterations.

4 Image Enhancement

It has been shown in [5] that the imaginary part of the isotropic complex diffusion can be applied to shock filter since the imaginary part contains the edge information of the real part. We consider the real part as the processed image of the target image. This characteristic of the imaginary part allows us to apply the imaginary part to edge-preserving smoothing as well as image enhancement. In the previous section, we have introduced the idea of image reconstruction. In the case of smoothing, θ has been set to be positive. According to Eq.(26), the diffusion of imaginary part behaves as edge smoothing due to the first term, where $\sin\theta$ is positive. On the other hand, negative θ makes Eq.(26) perform edge enhancement. Therefore, in order to enhance images, we reconstruct the image after every iteration with negative θ as was done in section 3.2.

Fig.5 shows the enhanced results with various parameters. Fig.5(a) is the original image, and Fig.5(b) and Fig.5(c) are the enhanced images with the parameters vales: $\beta = \frac{1}{2}$, and $\theta = -\frac{\pi}{6}$ and $\theta = -\frac{\pi}{3}$ respectively after 16 iterations. We can see that the edges are over-enhanced in Fig.5(c) due to the larger $\sin\theta$ of Eq.(26) than those in Fig.5(b). Also, the small value of β makes the diffusion flow less sensitive to edges and produces thick edges. Images in the bottom row of Fig.5 show enhancement results with $\beta = \frac{5}{6}$. The larger value of β results in sharper edges and more details.

5 Conclusion and Discussion

In this paper, we presented a novel formulation of complex diffusion for simultaneous image smoothing and edge enhancement. The formulation involved the use of an image graph representation as an embedded manifold, a novel image metric and a novel action functional yielding a new complex diffusion. Additionally, we developed a new quaternionic diffusion using this geometric framework for color images and demonstrated improved performance over the Beltrami flow. Comparisons were reported on data with added noise, using PSNR as a quantitative measure. Finally, we presented a "wavelet-like" interpretation of the complex diffusion. We interpreted the real and imaginary part of the complex diffusion as a low pass and high pass filter respectively and applied this concept to image reconstruction and enhancement. When performing the image reconstruction iteratively, we achieved faster convergence to the PSNR with positive θ and image enhancement with negative θ. Our future work will involve application of the proposed model to the complex-valued MRI data.

References

1. Kimmel, R., Sochen, N., Malladi, R.: From high energy physics to low level vision. In: ter Haar Romeny, B.M., Florack, L.M.J., Viergever, M.A. (eds.) Scale-Space 1997. LNCS, vol. 1252, pp. 236–247. Springer, Heidelberg (1997)

2. Sochen, N., Kimmel, R., Malladi, R.: A general framework for low level vision. IEEE Transaction on Image Processing, Special Issue on PDE based Image Processing 7(3), 310–318 (1998)
3. Kimmel, R., Malladi, R., Sochen, N.: Image as embedded maps and minimal surface: movies, color, texture, and volumetric medical images. International Journal of Computer Vision 39(2), 111–129 (2000)
4. Polyakov, A.M.: Quantum geometry of bosonic strings. Physics Letters 103B, 207 (1981)
5. Gilboa, G., Sochen, N., Zeevi, Y.Y.: Image Enhancement and Denoising by Complex Diffusion Process. IEEE Transaction on pattern analysis and machine intelligence (PAMI) 25(8), 1020–1036 (2004)
6. Gilboa, G., Zeevi, Y.Y., Sochen, N.A.: Complex Diffusion Process for image filtering. In: Kerckhove, M. (ed.) Scale-Space 2001. LNCS, vol. 2106, pp. 299–307. Springer, Heidelberg (2001)
7. Gilboa, G., Sochen, N.A., Zeevi, Y.Y.: Regularized Shock Filter and Complex Diffusion. In: Heyden, A., Sparr, G., Nielsen, M., Johansen, P. (eds.) ECCV 2002. LNCS, vol. 2350, pp. 399–413. Springer, Heidelberg (2002)
8. Liu, Z.-X., Lian, S.-G., Ren, Z.: Quaternion diffusion for color image filtering. J. comput. Sci. Technol. 21(1), 126–136 (2006)
9. Labunets, V.: Clifford Algebras as Unified Language for Image Processing and Pattern Recognition. NATO Advanced Study Institute, Computational Noncommutative Algebra and Applications, July 6-19 (2003), http://www.prometheus-inc.com/asi/algebra2003/papers/labunets2.pdf
10. Adler, S.L.: Quaternionic Quantum Mechanics and Quantum Fields. Oxford University Press, Oxford (1995)
11. El-Fallah, A.I., Ford, G.E., Algazi, V.R., Estes, R.R.: The invariance of edges and corners under mean curvature diffusions of images. In: Proc. Processing III SPIE, vol. 2421, pp. 2–14 (1994)
12. Perona, P., Malik, J.: Scale-space and edge detection usion ansiotropic diffusion. IEEE Trans. Pattern Anal. Machine Intell 12, 629–639 (1990)